D-^{3}He Protons as a Diagnostic for Target ρR

Areal density (ρR) is an important parameter for measuring compression in ICF experiments. Several diagnostics employing nuclear particles have been considered to deduce this quantity in implosions. One diagnostic is the knock-on deuterons,[1] i.e., deuterons produced by the elastic scattering of fuel deuterons and primary neutrons from the DT reaction. The number of knock-ons contained in the high-energy peak (typically 16% of the total produced) of the emergent spectrum is proportional to the fuel areal density [$(\rho R)_f$] and the position of the peak provides a measure of the plastic areal density [$(\rho R)_{CH}$]. This diagnostic, however, is limited to $(\rho R)_{CH} \sim$ 100 mg/cm^2 as higher compressions can considerably distort the emergent spectra, preventing a reliable interpretation of the signal.

For higher-density implosions, high-energy neutrons produced from the tertiary fusion reactions of the knock-on deuterons and tritons with the corresponding thermal fuel ions[2] have been considered as a diagnostic for fuel ρR. For instance, for "small" ρR (like those on OMEGA), the number of tertiary neutrons produced is proportional to $(\rho R)_f^2$, yielding a measure for the fuel areal density. However, since these neutrons are produced in tertiary reactions, their numbers are significantly lower relative to primary yields (typically by 5 to 6 orders of magnitude). This necessitates the development of new, sensitive neutron detectors.

An alternate technique for measuring high ρR is to use the primary protons from the D-^{3}He reaction, obtained by adding ^{3}He to the fuel. This diagnostic has the advantage that the charged-particle spectrometer for OMEGA,[3] currently being designed at MIT, can be used to detect the protons. In addition, these protons can serve as a diagnostic for cryogenic DD targets, which are being considered as initial cryogenic targets on OMEGA. DD targets do not have the drawbacks associated with the radioactivity of tritium and can be useful for standardizing laboratory techniques for cryogenics.

In what follows, we introduce the D-^{3}He proton diagnostic and set limits on the areal densities measurable through this method. We then examine the model dependence of this diagnostic by comparing results from a detailed time-dependent simulation and a simple model characterized by the conditions in the target around peak thermonuclear burn. This diagnostic is then discussed in the context of DT targets. Future areas of interest relating to this diagnostic will be discussed briefly.

The Diagnostic

The primary D-^{3}He protons are produced at an energy of 14.7 MeV from the reaction

$$D + {}^3He = \alpha + p(14.7 \text{ MeV}). \tag{1}$$

Protons lose energy as they traverse the target, and the energy loss of the emerging protons is proportional to ρR. Thus, unlike the knock-on diagnostic, which can provide a measure of the fuel and the tamper ρR individually, this diagnostic can be used to measure only the *total* ρR of the target. The interpretation of the signal can be complicated by the fact that this energy loss can be both temperature and density dependent.

Prior to its use on a cryogenic target, the D-^{3}He proton diagnostic can first be tested on current OMEGA gas targets. We demonstrate the diagnostic through a simple model for a typical gas target represented as a hot core (at 4 keV) surrounded by cold plastic (at 0.8 keV). The model serves to illustrate the limits of the diagnostic in terms of both ρR and temperatures in the target. We choose a fuel ρR of 30 mg/cm^2 corresponding to the typical fuel areal density during the time that the protons traverse the target in detailed 1-D simulations. The temperatures in the model are characteristic of the conditions during the peak thermonuclear burn. The emergent D-^{3}He proton spectrum, i.e., the normalized number of protons per unit energy interval, is shown in Fig. 73.22(a) for various values of plastic ρR. The figure shows the greater slowing down of the protons with increasing ρR of the plastic.

To examine the reliability of this diagnostic in the context of its sensitivity to temperatures in the target, we vary the electron temperatures in the plastic [Fig. 73.22(b)]. For a lower plastic

temperature the spectra are influenced only for lower proton energies (which occur for larger values of ρR). This can be easily explained through the energy-loss formulae that contribute to the spectrum.[4] We first note that the energy loss of the protons is dominated by losses to electrons. In addition, the D-^{3}He protons have much higher velocities than the electrons in the target for a wide range of energies and temperatures. In this regime, the thermal motion of the electrons can be ignored altogether. (The energy-loss mechanism is then through the excitation of collective plasma oscillations in the plastic.) For OMEGA targets the cold plastic can have temperatures of 1 keV or less and thus will have only a small effect on the spectrum of the very energetic protons.

Detailed simulations through the 1-D code *LILAC*[5] of the same target indicate that the maximum ρR achieved in the target is about 70 mg/cm^2 for the fuel and 170 mg/cm^2 for the plastic [Fig. 73.23(a)]. The protons, however, provide a
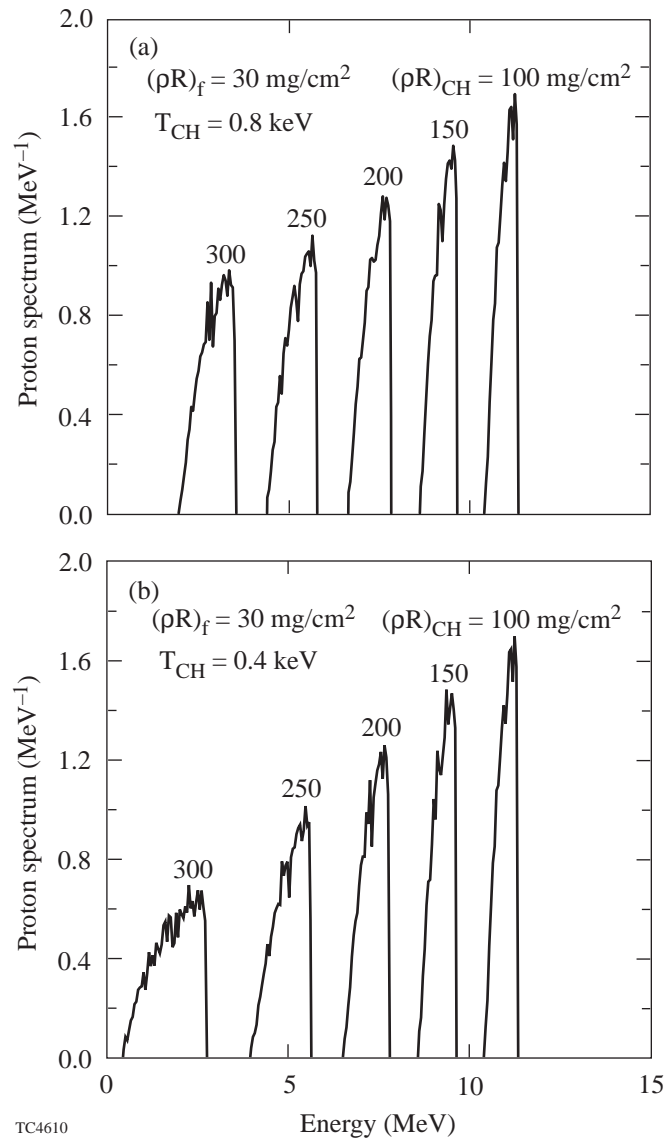
Figure 73.22

(a) Emergent D-^{3}He proton spectra (the normalized number of protons per unit energy interval) for the model (see text) with the choice of ρR as shown in the figure and with the plastic at a temperature of 0.8 keV. (b) Spectra of emergent protons with plastic at a temperature of 0.4 keV.
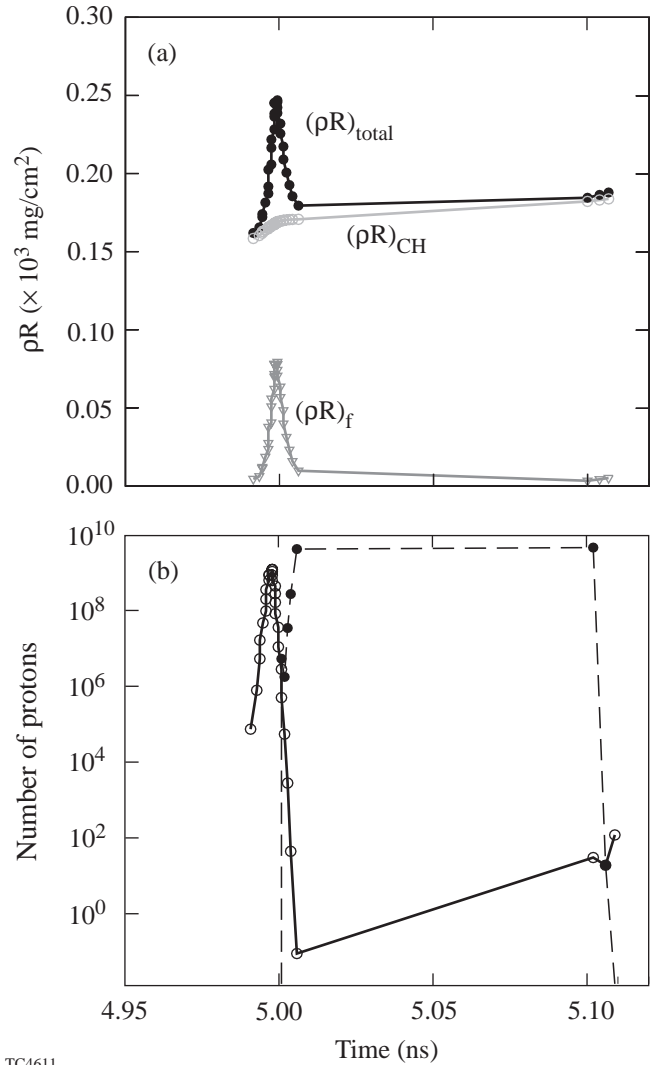
Figure 73.23

(a) Results from 1-D *LILAC* simulations for the ρR history of the target in Fig. 73.22(b); fuel ρR shown in triangles, plastic ρR shown in open circles, total target ρR shown in solid circles. (b) History of proton production in the target (open circles) and proton emission from the target (solid circles). The emergent protons measure an average total $\rho R \sim 200$ mg/cm^2.

measure of an average value of ρR, which is determined by the time that they traverse the target and can, in general, be less than the maximum value. Thus, by comparing the ρR history in Fig. 73.23(a), the history of proton production in the target [open circles in Fig. 73.23(b)], and the time history of protons exiting the target [solid circles in Fig. 73.23(b)], one can calculate the range of ρR measured through this diagnostic. The plastic ρR remains nearly constant at 170 mg/cm^2 during the time the protons traverse the target yielding this value as the average $(\rho R)_{CH}$. Furthermore, while a majority of the protons are produced near the peak value of $(\rho R)_f$ (70 mg/cm^2), they exit the target when the fuel ρR is lower (10 mg/cm^2), so that the protons sample a range of fuel ρR. Since the ρR of the plastic is so much larger than the average ρR of the fuel, the energy loss of the D-^{3}He proton should be characterized by $(\rho R)_{CH}$ in this example. The emergent proton spectrum from this simulation is shown in Fig. 73.24. One-dimensional time-dependent profiles obtained from *LILAC* were used as an input to the Monte Carlo particle-tracking code *IRIS*,[6] which calculated the spectrum emerging from the target. Since the detailed simulation indicates that the average $(\rho R)_{CH}$ measured by the protons is about 170 mg/cm^2, Fig. 73.24 must be compared with a model calculation (in Fig. 73.22) corresponding approximately to this value of the plastic fuel areal density. The comparison shows that the time-dependent evolution of the target has little influence on the position of the peak of the emergent proton spectrum. Both the model and the detailed

simulation peak at approximately the same energy. This feature will simplify the interpretation of an experimental signal; the position of the peak depends only on the knowledge of the fuel and plastic ρR. The width of the emergent spectrum, on the other hand, can depend on the details of the spatial profile of proton production, density, and fuel temperature history of the target. Even so, the energies at the FWHM of the spectrum provide a reasonable measure of the range of ρR in the target when compared to the model in Fig. 73.22. Some energy loss also takes place in the hot-fuel region. The low-energy tail is due to protons produced in the innermost regions of the hot fuel slowing down in the fuel, followed by energy loss in the plastic. For a target with lower fuel ρR, the slowing down in the fuel will be less significant and the range of ρR can be inferred more reliably. For larger $(\rho R)_f$, this model dependence must be constrained through comparisons of detailed simulations with simple models approximating conditions during thermonuclear burn.

The Diagnostic for DT Targets

The discussion thus far applies specifically to targets containing only deuterium and ^{3}He. The proton signal from these targets can be unambiguously identified as that due to the D-^{3}He proton. This signal is significantly larger than any other proton spectrum such as primary protons elastically scattered off fuel ions in the relevant energy region. We now discuss the diagnostic in the case where ^{3}He is added to the fuel that includes tritium in addition to deuterium.

Background related to the presence of tritium in the target is caused by the 14.1-MeV primary neutron from the DT reaction

$$D + T = \alpha + n(14.1 \ \text{MeV}). \tag{2}$$

One source of background arises from the elastic scattering of the 14.1-MeV primary DT neutrons off the protons in the plastic. The scattered protons have energies up to the maximum of 14.1 MeV.

Another important source of background arises when the 14.1-MeV neutron breaks up the deuteron in the reaction

$$D + n = 2n + p, \tag{3}$$

where protons are produced with energies up to 11.8 MeV.

Figure 73.24
Cumulative spectrum of D-^{3}He protons escaping the target from a 1-D simulation.

As seen in Fig. 73.22, the D-^{3}He proton spectrum can be significantly shifted downward due to energy losses in the

TC4612

target for the range of ρR expected in high-density implosions on OMEGA. The interpretation of the diagnostic proton spectrum can then be complicated by protons from the background mentioned above in the relevant energy range. Figure 73.25 shows the emergent proton spectrum from the earlier simple model representation [corresponding to Fig. 73.22(a) with $(\rho R)_{CH} = 150$ mg/cm^2] now being used for a gas target containing tritium in addition to deuterium and ^3He. The end point of the spectrum is at the maximum energy of the elastically scattered protons at 14.1 MeV. The proton background due to the deuteron breakup reaction is contained in Fig. 73.25 (and extends up to 4.5 MeV downshifted from the maximum of 11.8 MeV due to energy losses in the plastic). The D-^3He proton spectrum (whose range is shown as a dotted line) appears as an easily identifiable peak over the spectrum from the two sources of background mentioned above. A detailed simulation (not shown here) also shows the promise of this diagnostic for gas DT targets; the signal is somewhat broadened (with a width similar to Fig. 73.24) and is dominant over the background.

Several comments in the context of cryogenic targets are in order here. The background protons due to scattering in the plastic will be significantly reduced in this case because most
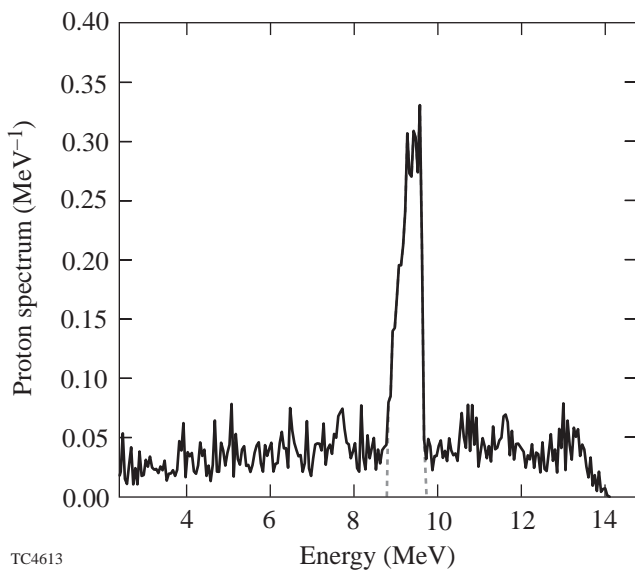
Figure 73.25
Spectrum of protons escaping a gas target containing DT and ^3He and modeled as described in the text. The peak is due to the D-^3He proton signal, and the background comprises protons from the deuteron breakup reaction and the elastic scattering of protons in the plastic. The dotted extension of the peak shows the range of the D-^3He proton signal.

TC4613

of the plastic will have been ablated from the target before thermonuclear burn.

In Fig. 73.26(a) we show the emergent proton spectrum from a 1-D simulation of an OMEGA cryogenic DT target. (The target comprises solid deuterium and tritium in a 1:1 ratio and encloses D-^3He gas. We ignore any confining plastic remnants that may exist during thermonuclear burn.) The D-^3He signal [shown as a dashed line in the region of its overlap with protons from the $(n,2n)$ reaction] extends from about 10 MeV to 14 MeV and is significantly broadened principally due to the time evolution of densities in the target. This dependence on the hydrodynamic evolution of the target can be constrained by comparing the emergent proton spectrum with that from a range of models similar to those used for the gas target in Fig. 73.22. However, the large $(n,2n)$ proton signal (about three orders of magnitude more protons are produced in the deuteron breakup reaction than in the D-^3He fusion) extends to about 11.8 MeV and makes the interpretation of the signal very dubious.

One possible method to lower this background is to include different proportions of deuterium and tritium in the solid fuel in order to reduce the yield of neutrons from the DT reaction and to reduce the numbers of protons from the $(n,2n)$ reaction. The proton spectrum from a target where the deuterium and tritium are in a ratio of 1:9 respectively is shown in Fig. 73.26(b). The number of background protons is significantly reduced, and the proton signal dominates in the region of overlap with the background. Thus, with some target optimization an unambiguous D-^3He proton signal can be obtained from cryogenic DT targets on OMEGA. In this context, tertiary neutrons mentioned earlier are a more attractive diagnostic for cryogenic DT targets because they have no background, place no constraints on the targets, and are applicable to higher densities.

Summary

In summary, the D-^3He proton spectrum is being considered as a means for inferring the total ρR of cryogenic DD targets. Using a gas target capable of achieving high areal densities, we have demonstrated that this diagnostic can be useful for up to $\rho R \sim 300$ mg/cm^2 for targets containing only D and ^3He. The reliability of this diagnostic is strengthened by its weak sensitivity to temperatures in the cold regions of the target for a wide range of ρR. For targets containing tritium, the interpretation of the signal is more difficult due to background arising from the 14.1-MeV primary DT neutron.
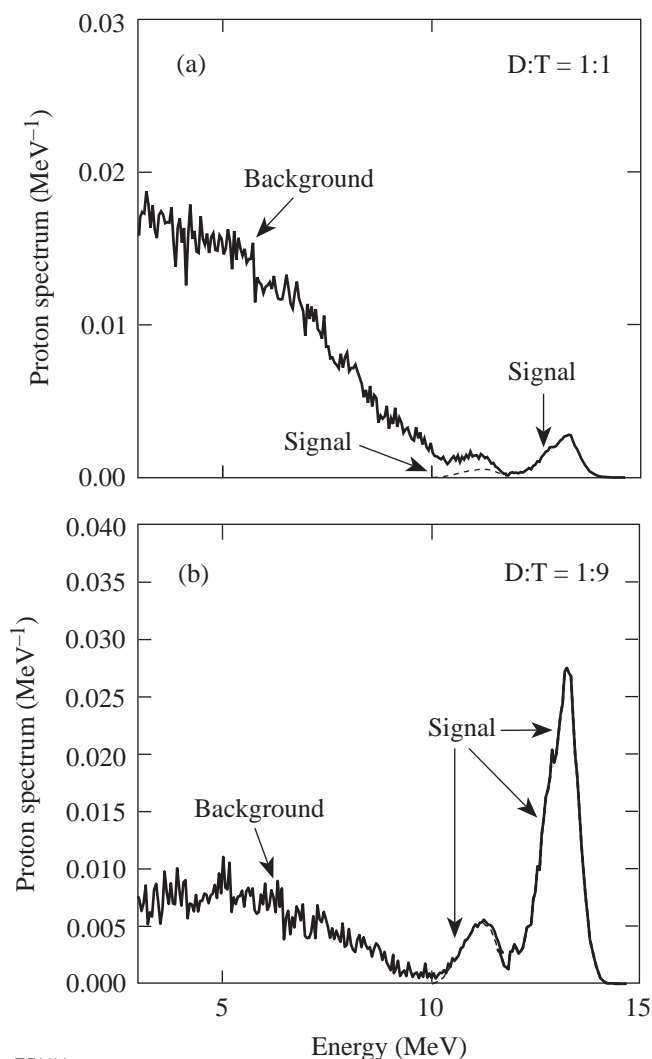
Figure 73.26

(a) Spectrum of emergent protons from an OMEGA cryogenic target with D:T = 1:1 in solid DT. D-^{3}He protons extend from about 10 MeV to 14 MeV. The dashed line is the extension of the signal in the region of its overlap with the background protons from the deuteron breakup reaction, which extends to 11.8 MeV. (b) Spectrum of protons from an OMEGA cryogenic target with D:T = 1:9.

Future Applications

This diagnostic could also serve as a method to measure gross asymmetries in the target that may arise due to energy imbalance in the beams, laser mispointing, etc. The D-^{3}He protons are produced isotropically, and any angular dependence of the proton yield or the spectrum is an indication of asymmetries in the target. Experimentally, track detectors placed strategically at various angles around the target could be used in conjunction with the charged-particle spectrometer to measure the various emergent proton spectra. Fuel areal densities could be inferred by comparing these spectra to calculations that include analytic angular variations in the target profiles. These measurements would track only gross variations in density (and temperature) constraining the calculations; inclusion of only "long"-wavelength perturbations to spherical symmetry should adequately model the emergent proton spectra. The Monte Carlo particle-tracking code *IRIS* is currently being modified with a view toward including such asymmetries in target profiles. Diagnostics for asymmetries in the target could then be developed.

REFERENCES

1. S. Skupsky and S. Kacenjar, J. Appl. Phys. **52**, 2608 (1981).

2. D. R. Welch, H. Kislev, and G. H. Miley, Rev. Sci. Instrum. **59**, 610 (1988). See also Laboratory for Laser Energetics LLE Review **69**, 46, NTIS document No. DOE/SF/19460-152 (1996). Copies may be obtained from the National Technical Information Service, Springfield, VA 22161.

3. D. G. Hicks, C. K. Li, R. D. Petrasso, F. H. Seguin, B. E. Burke, J. P. Knauer, S. Cremer, R. L. Kremens, M. D. Cable, and T. W. Phillips, Rev. Sci. Instrum. **68**, 589 (1997).

4. J. D. Jackson, *Classical Electrodynamics*, 2nd ed. (Wiley, New York, 1975).

5. *LILAC*, E. B. Goldman, Laboratory for Laser Energetics Report No. 16, University of Rochester (1973).

6. *IRIS*, S. Cremer, University of Rochester Laboratory for Laser Energetics (unpublished).